Biol. Cybern. 86, 343–353 (2002)
DOI 10.1007/s00422-001-0300-3

Biological Cybernetics

Dynamics and stability of legged locomotion in the horizontal plane: a test case using insects

J. Schmitt[1], **M. Garcia**[3,*], **R. C. Razo**[1,**], **P. Holmes**[1,2], **R. J. Full**[3]

[1] Department of Mechanical and Aerospace Engineering, Princeton University, Princeton, NJ 08544, USA
[2] Program in Applied and Computational Mathematics, Princeton University, Princeton, NJ 08544, USA
[3] Department of Integrative Biology, University of California, Berkeley, CA 94720, USA

Received: 17 April 2001 / Accepted in revised form: 20 November 2001

Abstract. Motivated by experimental studies of insects, we propose a model for legged locomotion in the horizontal plane. A three-degree-of freedom, energetically conservative, rigid-body model with a pair of compliant virtual legs in intermittent contact with the ground allows us to study how dynamics depends on parameters such as mass, moment of inertia, leg stiffness, and length. We find periodic gaits, and show that mechanics alone can confer asymptotic stability of relative heading and body angular velocity. We discuss the relevance of our idealized models to experiments and simulations on insect running, showing that their gait and force characteristics match observations reasonably well. We perform parameter studies and suggest that our model is relevant to the understanding of locomotion dynamics across species.

1 Introduction

The spring-loaded inverted pendulum (SLIP) or spring–mass monopode model has proved useful in unifying and explaining the mechanics of legged locomotion in the sagittal plane for animals ranging from 2.5 g cockroaches to 85 kg rams, encompassing bipeds to 44-legged centipedes that employ trotting, running, and hopping gait patterns (McMahon 1984; McMahon and Cheng 1990; Blickhan and Full 1993; Farley and Gonzalez 1996; Farley and Morgenroth 1999; Anderson 2000). In this paper we describe a similar, simplified, lateral leg-spring (LLS) model for dynamics and stability in the horizontal plane. While it was developed with sprawled-posture animals such as insects in mind, and is applied here to the cockroach as a test case, we believe it can serve as an exemplar for stability and gait studies of other species. It shares the simplicity of the SLIP, but includes inertia effects to account for yawing motions. Ultimately we wish to integrate horizontal- and sagittal-plane dynamics in a coupled system.

The present paper follows Schmitt and Holmes (2000a,b, 2001), in which the LLS model was developed and analyzed, preliminary comparisons with experimental data were made, and stability analyses carried out. Here we provide detailed comparisons with data from rapidly running cockroaches of the species *Blaberus discoidalis*, and perform parameter variation studies with a view to assessing the model's ability to account for variability both within and across species. After describing the model in Sect. 2, we: (1) explicitly define stability and provide measures of performance (Sect. 3), (2) estimate parameters for a specific insect as a test case and assess how well the model captures and explains steady gaits over a range of speeds including the preferred speed (Sect. 4), and (3) consider geometric size scaling and determine how individual parameter variations affect performance (Sect. 5). The results are discussed and assessed in Sect. 6.

2 The lateral leg-spring model

The LLS model, illustrated in Fig. 1, and described in detail in Schmitt and Holmes (2000b), consists of a rigid body of mass m and moment of inertia I (in insects, the head–thorax–body unit), that is free to move in the plane under forces generated by two massless, laterally rigid, axially elastic legs, pivoted freely at a point P (generally displaced forward or backward from the center of mass (COM) G), and intermittently contacting the ground at feet F, F' with a 0.5 duty cycle. F, F', and P are pin joints (i.e., with no torques). In considering multilegged animals, we appeal to the stereotyped use of a double-tripod gait in hexapods, and a double-quadruped gait in crabs

Correspondence to: P. Holmes
Present addresses:
* Borg-Warner Automotive, 770 Warren Road, Ithaca, NY 14850, USA
** Silicon Valley Group, Inc., 77 Danbury Road, M/S 470, Wilton, CT 06897, USA

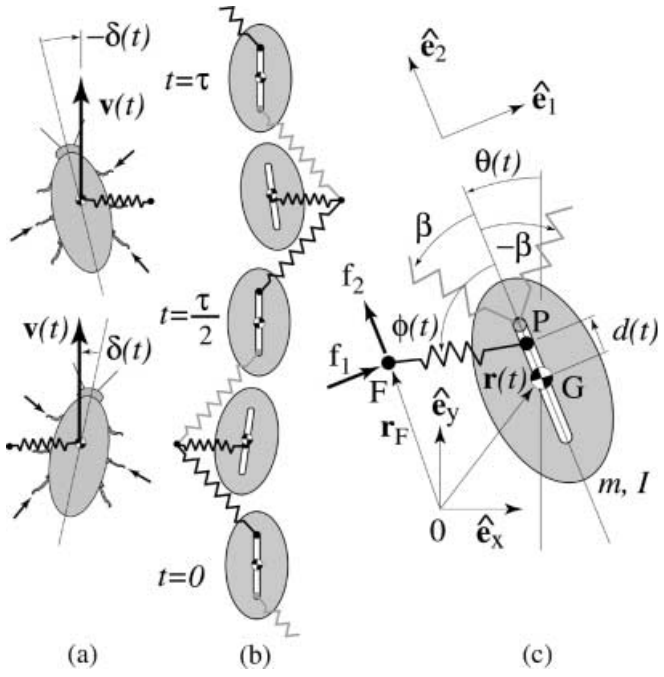

Fig. 1a–c. Overhead views of a cockroach (**a**), a cartoon of the lateral leg-spring bipedal model during one stride of period τ (**b**), and model details (**c**). O denotes a fixed 'origin' on the ground, F is the current foot position F' (not shown) is the next foot position on the opposite side of the body, and G is the body center of mass (COM). P is the leg attachment point (also called center of pressure, COP) which may move or be fixed with respect to G according to the prescribed position function $d(t)$. f_1 and f_2 are components of force generated in the leg with respect to body axes e_1, e_2; $r(t) = (x(t), y(t))$ is the mass-center position with respect to inertial frame e_x, e_y. $\theta(t)$ is the body orientation, and $\phi(t)$ is the leg angle relative to body. The leg positions with respect to the body at the start of each step are sketched in gray; $\pm\beta$ is the leg angle with respect to the body centerline at touchdown. $\delta(t)$, shown in **a**, is the angle of the mass center velocity $v(t)$ with respect to the body centerline

(Blickhan and Full 1987). Errors induced by collapsing leg groups linked in such stance phases to a single virtual leg are discussed in Sect. 4.

A full stride begins at left touchdown at time $t = t_n$ with spring relaxed at leg angle $\phi = +\beta$ relative to body orientation; the left stance phase ends when the spring is again relaxed, the body having 'run past its foot.' At this instant (t_{n+1}) the left leg is raised to begin its swing phase and the right leg is set down at angle $-\beta$; its stance phase, and the stride, ends with spring relaxation at right liftoff/left touchdown. Choosing a linear spring, the model is entirely characterized by six physical parameters: leg stiffness, k, and relaxed length, l, the pivot position relative to the COM, d, along with m, I, and β. Balancing the linear and angular momentum results in three equations of motion for COM translation $\boldsymbol{r}(t) = (x(t), y(t))$ and body orientation $\theta(t)$ during stance:

$$m\ddot{\boldsymbol{r}} = \mathbf{R}(\theta(t))\boldsymbol{f}, \quad I\ddot{\theta} = (\boldsymbol{r}_{\mathrm{F}}(t_n) - \boldsymbol{r}) \times \mathbf{R}(\theta(t))\boldsymbol{f}\ , \tag{1}$$

where $\mathbf{R}(\theta)$ is the rotation matrix, needed to transform leg forces $\boldsymbol{f}$ (relative to the body) to the inertial frame; $\boldsymbol{r}_{\mathrm{F}}(t_n)$ denotes touchdown foot position, expressed via d, l, β, and body angle $\theta(t_n)$ at touchdown, and $\times$ denotes the vector cross product. Normalizing length with respect to l and nondimensionalizing time $\tilde{t}$, the parameters reduce to four nondimensional groups:

$$\tilde{k} = \frac{kl^2}{mv^2},\ \tilde{I} = \frac{I}{ml^2},\ \tilde{d} = \frac{d}{l},\ \text{and } \beta;\ \text{with } \tilde{t} = \frac{vt}{l}\ . \tag{2}$$

Here v is a representative speed (e.g., COM velocity magnitude at touchdown, or average forward speed $\langle v \rangle$) and $\sqrt{\tilde{k}}$ is a Strouhal number characterizing the ratio of storable potential to kinetic energy. For fixed $\tilde{k}, \tilde{I}, \tilde{d}$, and β, solutions of (1) describe *identical* paths in (x, y, θ) space, scaled by l, at rates determined by $\tilde{t}$.

Global conservation of total energy, and conservation of angular momentum about the foot in each stance phase assist in integration of (1), complete accounts of which appear in (Schmitt and Holmes 2000b). At touchdown/liftoff the foot position instantaneously switches to $r_{\mathrm{F}}(t_{n+1})$, and integration continues. Simple codes may be written for numerical simulations in, for example, the MATLAB environment.

The 'hip pivot' P may be fixed, or may move dependent on leg angle ϕ relative to body; the rule

$$d = d_0 + d_1\left(\phi - \frac{\pi}{2}\right) \tag{3}$$

exemplifies both cases ($d_1 = 0$, fixed; $d_1 \neq 0$, moving). The latter *moving center of pressure* (COP) protocol can better reproduce torques resulting from variations among individual foot forces. (Specified torques could also be applied at P: see Schmitt J and Holmes P, unpublished work, 2002) Moreover, in place of passive, SLIP-like force generation resulting from leg compression in which $\boldsymbol{f}$ derives from a potential function depending on leg length $(\boldsymbol{r} - \boldsymbol{r}_{\mathrm{F}}(t_n))$, leg forces $\boldsymbol{f}(t)$ may be wholly prescribed as functions of time, or via combinations of these limiting, 'event-driven,' and 'clock-driven' strategies. In fact the prescribed force studies of Kubow and Full (1999), in which representative forces were applied at foot positions, motivated the present generalized models, which we believe are better suited to represent the effects of mechanical feedback or 'preflexes' in gait stabilization. Further information and detailed analyses of these models appear in Schmitt and Holmes (2000b, 2001).

3 Steady periodic gaits

3.1 Families of gaits and stability

The dynamical behavior of the model (1) is conveniently described in terms of touchdown values of COM velocity magnitude $v(t) = |v(t)| = |\dot{\boldsymbol{r}}(t)|$ and COM velocity heading $\delta(t)$ relative to body axis, body orientation, or yaw angle $\theta(t)$ relative to a fixed reference frame, and body angular velocity $\dot{\theta}(t) \equiv \omega(t)$; see Fig. 1. Integration of (1) (Schmitt and Holmes 2000b) produces a stride or *step map* $\mathbf{F}$ specifying these variables at each touchdown instant $t = t_{n+1}$ in terms of their values at the preceeding touchdown $t = t_n$:

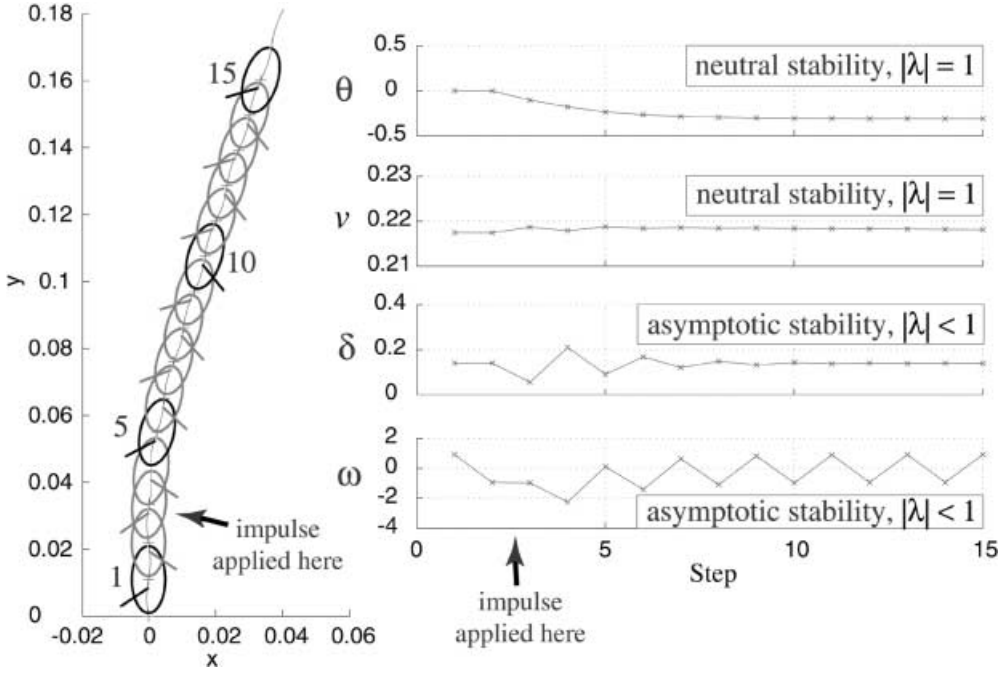

Fig. 2. Response to perturbations and stability explanation. The cartoon shows the model recovering from a perturbation to a stable gait ($v = 0.2175, \delta = 0.14, \theta = 0, \omega = -0.9295$ with parameters $k = 2.25, m = 0.0025, I = 2.04 \times 10^{-7}, d = -0.0025, \beta = 1$) applied at the beginning of the third step. The graphs show the state variables at the beginning of each step. The model is neutrally stable in θ and v (corresponding eigenvalues $|\lambda|$ of unit magnitude) but asymptotically stable in ω ($\equiv \dot{\theta}$) and δ; the corresponding eigenvalues are less than one in magnitude. Note that ω changes sign with each step and so is not expected to decay to a straight line as the other state variables do; the same might be true for θ, except that this particular solution has fixed points at $\theta =$ constant

$$(v_{n+1}, \delta_{n+1}, \theta_{n+1}, \omega_{n+1}) = \mathbf{F}(v_n, \delta_n, \theta_n, \omega_n) \ , \qquad (4)$$

where $v_n = v(t_n)$, etc. Here we retain the terminology of Schmitt and Holmes (2000a,b). In traditional biological usage, heading denotes the COM velocity with respect to compass direction (i.e., the quantity $\delta + \theta$), and body orientation denotes the angle the body makes with the velocity vector (δ).

In a steady periodic gait $v_{n+1} = v_n = \bar{v}$ etc., corresponding to a fixed point of $\mathbf{F}$. For stable gaits, the variables converge toward constant values: $\delta_n \to \bar{\delta}$, etc.; see Fig. 2. Convergence rates are determined by the *eigenvalues* λ_j of the 4×4 Jacobian matrix of first derivatives of $\mathbf{F}$: perturbations decay at the rate $|\lambda_j|$ per stride. Two eigenvalues are necessarily unity, corresponding to neutral speed (v) and orientation (θ) stability due to energy conservation and rotational symmetry: if all remaining $|\lambda_j| < 1$, we have stability; if any $|\lambda_j| > 1$, we have instability and perturbations grow.

The model displays periodic gaits with fore–aft, lateral, and yaw oscillations. Figure 3 shows gait families for the fixed- and moving-COP models illustrating how $\delta, \theta, \dot{\theta} \equiv \omega$, and the relevant eigenvalue magnitude $|\lambda|$ depend on v; all other parameters (m, I, l, d, k, β) are fixed. In all cases a saddle-node bifurcation (Guckenheimer and Holmes 1983) occurs at a critical COM speed $v = v_c$ (or $\tilde{k} = \tilde{k}_c$), below which no gaits exist and above which two branches emerge, one potentially stable with relatively small lateral and yaw oscillations (small $|\delta|$), and one with large oscillations (large $|\delta|$), which is typically unstable. (Bifurcation theory (Guckenheimer and Holmes 1983) implies that in general at most one branch may be stable, but both *could* be unstable.) For this model, with passive compliant spring legs and fixed COP, the smaller $|\delta|$ gaits exhibit relative heading and angular velocity stability if $d < 0$ (hip behind COM), and instability for $d > 0$; moving-COP gaits are stable

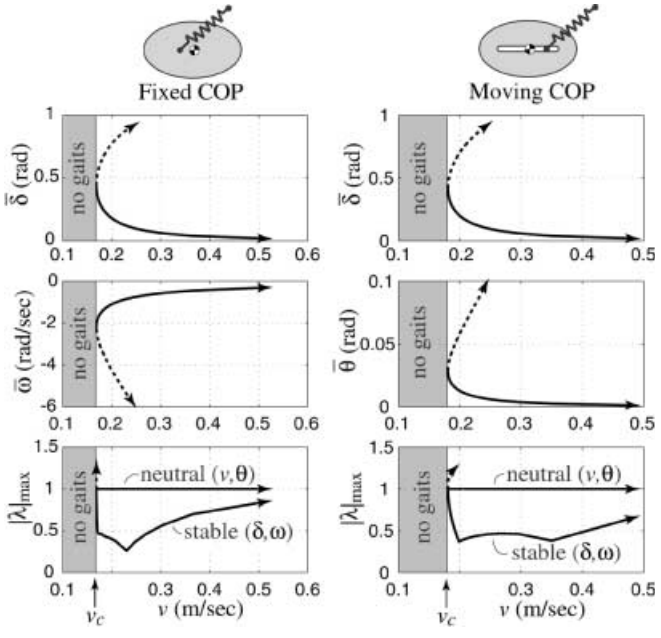

Fig. 3. Families of periodic gaits for the fixed- and moving-COP models with parameters characteristic of *Blaberus discoidalis*. From *top* to *bottom* the panels show COM velocity vector direction δ, body angular velocity $\omega \equiv \dot{\theta}$, and body orientation θ at touchdown, and eigenvalue magnitudes $|\lambda|$. See Sect. 4 for parameter values. (For fixed COP $\theta =$ const. at touchdown; for moving COP $\omega = 0$ at touchdown: hence our display of ω and θ.) Stable branches are shown *solid*, and unstable branches are *dashed* (only the neutral and least stable eigenvalues are shown). Note critical speed v_c below which gaits do not occur, neutral eigenvalues $|\lambda| = 1$ corresponding to speed v and orientation θ, and maximal $|\lambda| < 1$ corresponding to COM heading δ and angular velocity ω decay rates, and the stability optima for $v \approx 0.23$ and $0.20 < v < 0.34$ m s^{-1}, respectively

provided d moves backward during stance ($d_1 < 0$ in Eq. 3), as shown in Fig. 1b. Stability results from losses/gains of angular momentum incurred in leg-to-leg

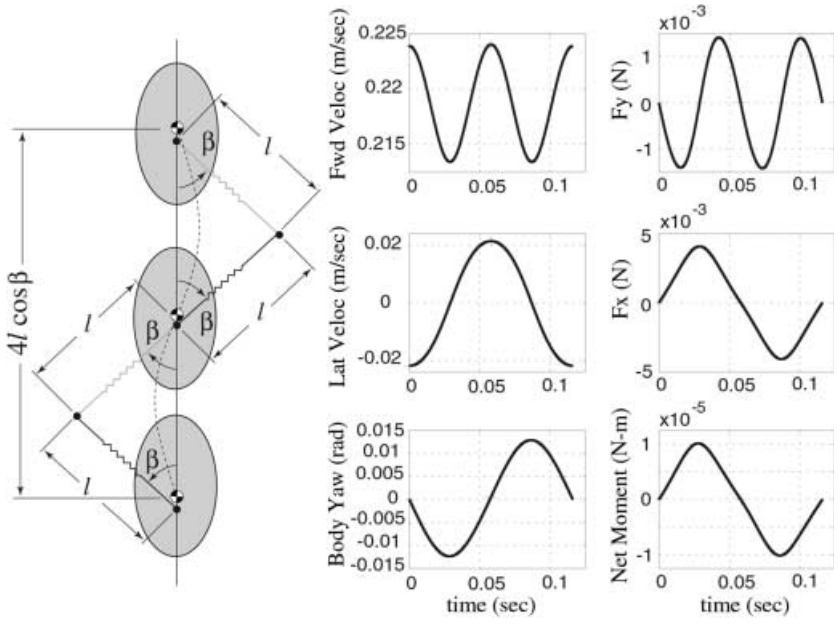

Fig. 4. COM path, velocity, yaw, and leg force and body moment variations for steady gait of the fixed COP, spring-leg model with parameters characteristic of *Blaberus discoidalis* running at the preferred speed 0.22 m s^{-1}. See Sect. 4 for parameter values

transit. Note that minima in $|\lambda|$, corresponding to stability optima, occur around $0.2 < v < 0.3$ m s^{-1} in Fig. 3.

Since energy is conserved, there is *neutral* speed stability: a one-parameter family of gaits exists over a range of forward speeds. Owing to the neutral eigenvalues, typical perturbations result in adoption of a 'new' gait at a different speed and orientation: the model returns to running with COM position, heading, and orientation oscillating stably about a new path; hence we term the heading and body angular velocity stability *relative* (for further details, see Schmitt and Holmes 2000a,b). These results show that purely mechanical 'preflexes,' with a simple 'feed forward' leg touchdown/liftoff protocol requiring minimal sensing, can yield stable straight running. In Schmitt and Holmes (2000a) it is also shown that turns can readily be obtained by transient changes in d applied over two strides.

3.2 Performance measures

The gaits pictured in Fig. 3, and Figs. 4–6 below, show variations in fore–aft and lateral velocities and forces, moments, and yaw angles throughout the stride. From these time-dependent functions we extract four gross *performance measures*. The *maximum relevant eigenvalue* $|\lambda| < 1$ is perhaps the most important, since it characterizes the animal's resistance to perturbations with respect to all variables, which decay at least at the rate $|\lambda|$ per stride. The COM velocity at which $|\lambda|$ achieves its minimum then suggests a *preferred speed* V. We take $|\delta|$, the *COM heading angle relative to body orientation*, as a second performance measure; it characterizes the relative degree of lateral oscillation of the body. $|F|$, the *peak leg force* which is available in many animal data sets, provides a third measure, and $|\theta|$, the *peak yaw angle deviation* (or $|\omega|$, the *peak angular velocity*), is a final performance measure.

4 Comparison with *Blaberus discoidalis* gaits

4.1 Parameter estimates

Parameters characteristic of the death-head cockroach *Blaberus discoidalis* were selected (Full and Tu 1990, 1991): $m = 0.0025\,\text{kg}, I = 2.04 \times 10^{-7}\,\text{kg m}^2, l = 0.01\,\text{m}, d = -0.0025\,\text{m}, k = 2.25 - 3.5\,\text{N m}^{-1}$, and $\beta = 1$ radian (57.3°). I and m may be directly measured, and choices of l and β are constrained by the requirement that stride length $L_s = 4\cos\beta \approx 0.022\,\text{m}$; see Fig. 4. Stiffnesses were chosen, via $\tilde{k}_c$, to given a reasonable average forward speed range for steady gaits (above $\langle v \rangle \approx 0.15\,\text{m s}^{-1}$), and to ensure that leg compressions at midstride were not excessive.

4.2 Blaberus at the preferred speed

Figures 4 and 5 show typical COM path and velocity, body angle, and fore–aft and lateral forces and moments in steady gait for the fixed- and moving-COP models; analogous data from experimental trials are shown in Fig. 6.

It is immediately striking that the phased oscillatory fore–aft and lateral force and velocity patterns produced by the passive leg springs closely resemble those observed in cockroaches (e.g., Full and Tu 1990; Full et al. 1991; Kram et al. 1997): compare the top four panels of Figs. 4–6. However, the fixed-COP model (Fig. 4) produces yaw oscillations of sinusoidal rather than the observed cosinusoidal form, due to body torques incurred by the fixed 'hip.' This is remedied by allowing a moving COP, as in Fig. 5, for which d was specified by (3), resulting in variation of $d = \pm 0.002$ m: compare the bottom panels of Figs. 5 and 6. For these computations, we took $l = 0.008$ m and $k = 3.52$ N m^{-1}; again l and β are constrained by the stride geometry; see Fig. 5.

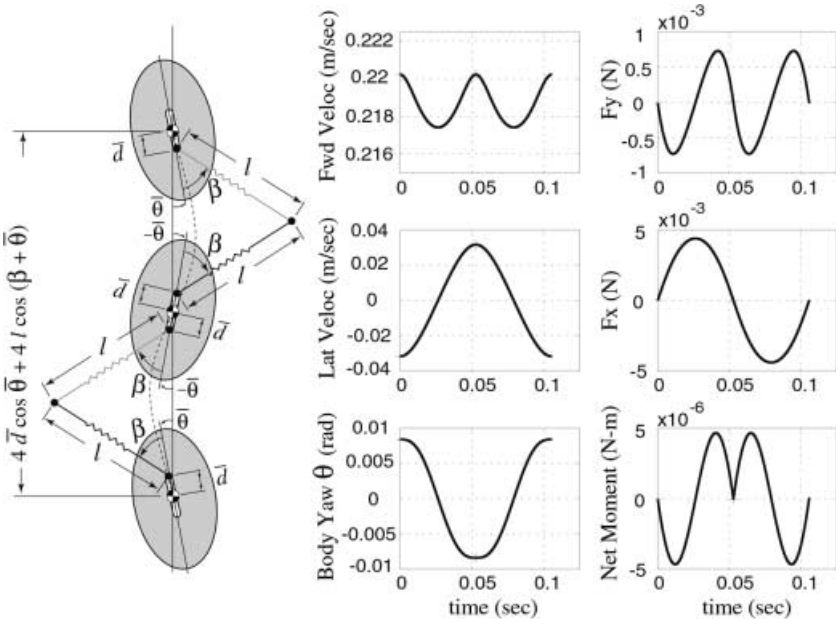

Fig. 5. COM path, velocity, yaw, and leg force and body moment variations for steady gait of the moving-COP, spring-leg model with parameters characteristic of *Blaberus discoidalis* running at the preferred speed 0.22 m s^{-1}. The stride-length formula in the sketch assumes that $d(t)$ varies symmetrically between $\bar{d}$ and $-\bar{d}$. $\bar{\theta}$ is the value of θ at leg touchdown. See Sect. 4 for parameter values

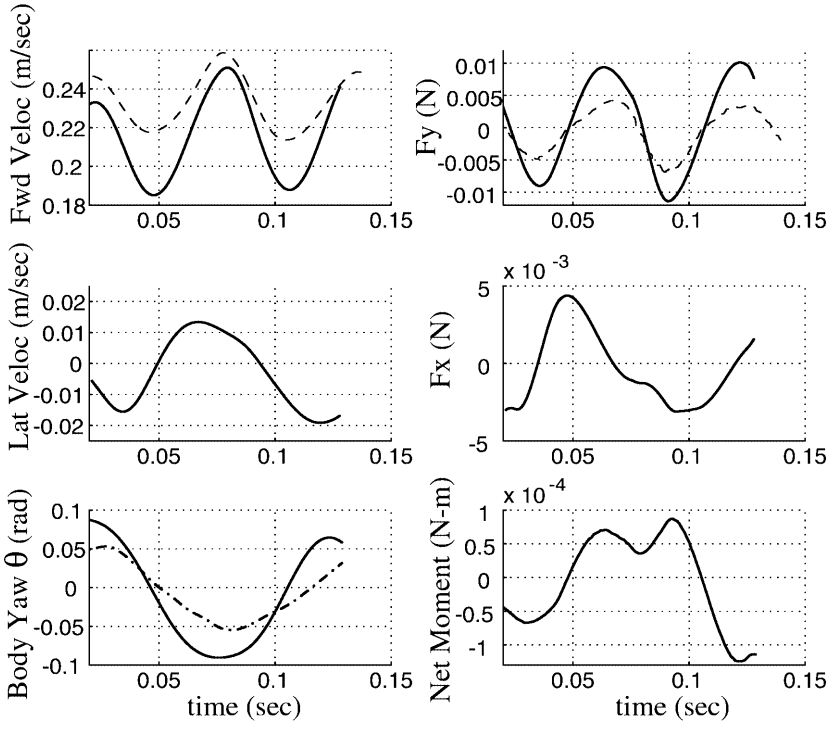

Fig. 6. Velocity, yaw, leg force, and moment variations over approximately one stride for *Blaberus discoidalis* moving at 0.22 m s^{-1}. The sign convention is the same as for the models. Data for all components from a single trial (Full et al. 1991; Kram et al. 1997) are shown *solid*, with yaw angle computed from net moments; the direct kinematic yaw measurement is *dashed-dotted*. The *top panels* also show as *dashed curves* fore–aft force and velocity data from a different trial (Full and Tu 1990), to illustrate variation in magnitudes and average speed (stride durations are adjusted to match). Since lateral forces were not simultaneously measured in Full and Tu (1990), moments could not be computed, but they do exhibit less variability

Quantitative comparisons of lateral force and velocity magnitudes are good, with model values being $\approx 30\%$ higher than experimental values. Model fore–aft magnitudes differ more appreciably, being lower than experimental by factors of 2–10 when compared over a large data set (Full and Tu 1990; Full et al. 1991, Kram et al. 1997). However, we note that there is significant variation among trials of individual animals, and among animals, even after scaling to the mass value ($m = 0.0025$ kg) used in the model. The data shown as solid curves in Fig. 6 were reconstructed for a typical run of one animal as in Garcia M, Full R, Kram R, Wong B, unpublished work, 2001, from trials of Full et al. (1991) and Kram et al. (1997) These data were selected for their clean phase relationships, although the fore–aft values are unusually high, and we include fore–aft data from Full and Tu (1990) for a second animal, closer to the mean values adopted in Kubow and Full (1999), to illustrate the variability.

We also note that the LLS model describes only horizontal plane dynamics, while Fig. 6 is derived from full three-dimensional motions. This may account for the underestimate of fore–aft forces and velocity variations by our models. Moments and yaw angles are

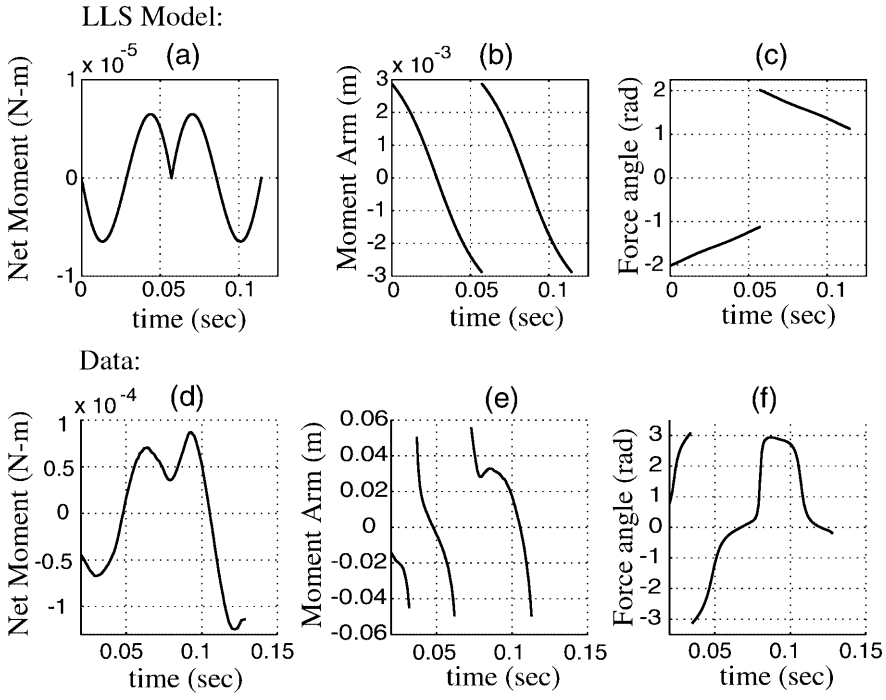

Fig. 7a–f. Moment (**a**), moment arm (**b**), and orientation of force vector relative to body axis (**c**) through left and right strides for the moving-COP model compared with results from the data of Fig. 6 (**d–f**). The moment arm was found by calculating the net force and moment on the body at each instant and then calculating the position along the body centerline where the net force must act in order to produce the net moment

significantly lower than observed (by factors of 10–20); we ascribe this primarily to the collapse of the leg support tripod to a single virtual leg, as described in Sect. 4.3.

With the provisos noted here, we conclude that the LLS model, with appropriate parameters, can reasonably capture the dynamics of one insect species. We have already noted that it explains the robustly stable running behavior of typical insects in purely mechanical terms and allows one to rationally define a preferred speed at which the performance measure $|\lambda|$ achieves its minimum, corresponding to optimal stability with respect to all variables. Referring to Fig. 3, this occurs in the range $0.2 < v < 0.3$ m s^{-1}, as observed for *Blaberus*.

4.3 Tripod versus an effective leg

Any system of varying forces in the plane can be reduced, at each instant, to a single resultant force and moment acting at the COM (Meriam and Kraige 1997), but these may not correspond to forces directed from 'feet' F and F', fixed in inertial space, to a 'hip,' P, attached to the moving body, throughout the stance phase. We have already noted that the fixed-COP model fails to reproduce experimentally observed moments and hence that yaw oscillations display incorrect phasing. Here we consider how well the moving-COP model reproduces trial data from running cockroaches (Full and Tu 1990; Full et al. 1991; Kram et al. 1997). The moment at the COM, effective moment arm $d(t)$, and resultant force vector orientation relative to the body for model and trial data are compared in Fig. 7.

Experimental quantities were computed by summing the moments due to individual foot forces (Ting et al. 1994). Note that while $d(t)$ behaves *qualitatively* as in the moving-COP simulation of Fig. 5, its magnitude is significantly higher; indeed, at touchdown and liftoff, $|d|$ exceeds the insect's body length. In the model, $d_{\mathrm{TD}} = 0.4l$, and, as noted above, increases in parameter d_1 of (3) lead to an oscillatory yawing instability associated with a low I/d value. The model is thus incapable of producing the larger moment variations characteristic of the animal.

Figure 7 also reveals that the direction of the resolved tripod forces relative to the body axis varies significantly more than the leg angle for our bipedal model, being oriented at $\approx \pm 20^{\circ}$ and $\pm 160^{\circ}$ at touchdown and liftoff, respectively. We conclude that the tripod support phase provides greater flexibility in moments and forces than a single passive virtual leg affords.

4.4 Gait variation with speed

If all physical parameters remain constant, then $\tilde{k}$ drops as $v^{-2} \approx \langle v \rangle^{-2}$ with increasing speed. The resulting decrease in lateral, fore–aft and yaw velocity variations leads to a drop in maximum foot forces; see Fig. 8c. Experimental evidence suggests instead an increase in force magnitude of about 100% in the speed range 0.05 to 0.55 m s^{-1}. This implies that the virtual leg stiffens and/or lengthens as $\langle v \rangle$ increases, leading to a slower reduction in $\tilde{k}$. (Holding $\tilde{k}$ constant would lead to a quadratic force increase with speed, via the time rescaling: this is much greater than observed.) Moreover, fixed l and β, in particular, imply fixed stride length and linearly increasing stride frequency, so in order to reproduce the stride length/frequency data of (Ting et al. 1994, Fig. 2; see Fig. 8a,b), we must adjust one or both of these parameters in the range $\langle v \rangle \geq 0.25$ m s^{-1}.

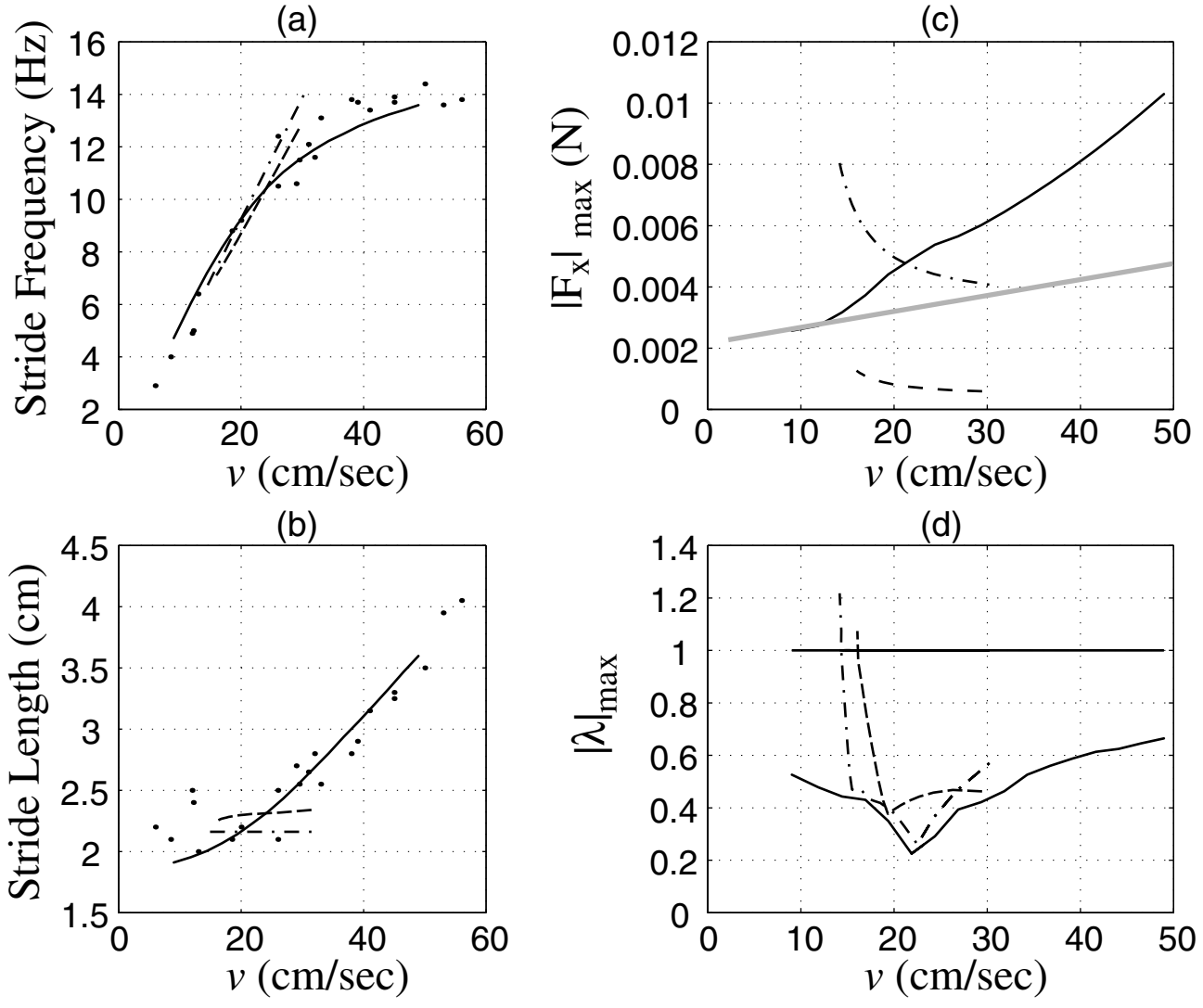

Fig. 8. **a** Leg cycle frequency f_s, **b** stride length L_s, **c** maximum lateral force $|F_x|_{max}$ variations, and **d** maximum eigenvalue magnitude $|\lambda|_{max}$ with speed for the fixed- and moving-COP spring-leg models with parameters characteristic of *Blaberus discoidalis*. *Dashed-dotted lines*, fixed COP; *dashed lines*, moving COP; both with constant physical parameters. *Solid curves*, fixed COP with varying parameters as described in text. *Filled circles* are observations from Ting et al. (1994) and the *thicker gray line* in **c** is an estimate of lateral forces from animal data (rescaled for $m = 0.0025$ kg), as explained in the text

We propose that increasing muscle activity with speed leads to modest increases in k, and, at higher speeds, for which muscle contraction rates may provide frequency limits, increases in l and/or decreases in β result from joint angle changes. We therefore constructed a family of gaits over the speed range $0.10\,\mathrm{m\,s^{-1}}$ to $0.55\ \mathrm{m\,s^{-1}}$ by allowing stiffness k to increase linearly with speed from $1\ \mathrm{N\,m^{-1}}$ to $2.25\,\mathrm{N\,m^{-1}}$, as $\langle v \rangle$ rises to $0.25\ \mathrm{m\,s^{-1}}$, remaining fixed thereafter, and increasing l from 0.0092 m to 0.0121 m and decreasing β from 1.3 radians to 0.73 radians throughout the entire speed range. The latter were varied linearly above $0.25\ \mathrm{m\,s^{-1}}$, and slightly more slowly from $0.1\,\mathrm{m\,s^{-1}}$ to $0.25\,\mathrm{m\,s^{-1}}$ (keeping them constant in this range led to nonsmooth stride-length and frequency curves, with frequency *decreasing* above $0.25\,\mathrm{m\,s^{-1}}$). The 20–30% variations lie within those observed in running insects (Jindrich and Full 1999). The lower limit for k was dictated by the requirement that $v_c < 0.1\,\mathrm{m\,s^{-1}}$. Figure 8 shows the results of this procedure for the fixed-COP model, along with fixed parameter studies for both fixed- and moving-COP cases. We also show the maximum lateral force magnitudes in comparison with estimates from experimental data of Full et al. (1991) To create this estimate, we used force data from single legs (normalized by animal weight) to fit a curve of maximum lateral force as a function of speed *for each leg*, and then summed the predicted leg forces to estimate the whole-body lateral force as a function of velocity.

We also note that the physical parameter variations employed to produce the matched data of Fig. 8 result in improved stability: the (largest-magnitude) eigenvalue remains nearer its minimum over a wider speed range than for constant parameter values: compare Fig. 8d with the eigenvalue plots of Fig. 3. Thus, tuning spring constant, leg length, and touchdown angle results in

Table 1. Summary of parameter scaling effects on gait. The new performance measures are equal to the appropriate column entry multiplied by the old ones, depending on whether k, m, l, or I/d changes. The scale factors are computed as follows: $R_m = m_2/m_1$, $R_k = k_2/k_1$, $R_l = l_2/l_1$, and $R_d = I_2 d_1/I_1 d_2$. Stiffness scaling (k) is exact, while mass (m), length (l), and inertia/pivot (I/d) scalings are good approximations over a reasonable parameter range. Note that the scaling effects can be superimposed linearly to determine the effects of changing several parameters

New	Pure geom	$k_1 \to k_2$ alone	$m_1 \to m_2$ alone	$l_1 \to l_2$ alone	$I_1/d_1 \to I_2/d_2$ alone	Old
λ_2 =	1	1	See text	See text	See text ×	λ_1
δ_2	1	1	1	1	≈1	δ_1
F_2	R_m	R_k	1	R_l	1	F_1
θ_2	1	1	R_m	R_l	R_d^{-1}	θ_1
ω_2	$R_m^{-1/6}$	1	$R_m^{1/2}$	R_l	R_d^{-1}	ω_1
V_2	$R_m^{1/6}$	$R_k^{1/2}$	$R_m^{-1/2}$	R_l	1	V_1

superior stability over the speed range than could be obtained were these parameters to remain fixed. Similar observations can be made when parameters are varied in the Kubow–Full model (Kubow and Full 1999).

5 Parameter dependence and scaling

For the results presented above, we estimated and then fixed parameters. We now ask how parameter changes with respect to those chosen for the cockroach affect performance, and establish plausible ranges for the nondimensional parameters of (2). We first consider the effects on model gaits of geometrical scaling (McMahon 1984), in which physical parameters change in concert, and then examine the effects of individual variation. More extensive studies appear in Schmitt and Holmes (2001, Sect. 3).

5.1 Geometric scaling

For geometrically similar animals, $m \sim l^3$ and $I \sim l^5$. If we additionally assume that preferred speed scales with Froude number (McMahon 1984), so $v^2 \sim gl$, and that leg stiffness scales as $k \sim l^2$ (McMahon 1984), then the nondimensional parameter vector $\tilde{\mu} = (\tilde{k}, \tilde{I}, \tilde{d}, \beta)$ of (2) remains constant and $t \sim \sqrt{l}\,\tilde{t}$. (Note that this is based on A.V. Hill's proposal (Hill 1950) that muscle force $ml/t^2 \sim l^2 v^2$ scales as kl, and the use of $v^2 \sim gl$. Elastic similarity yields the same result (McMahon and Bonner 1983; Blickhan and Full 1993)). Such animals should therefore display similar fore–aft, lateral, and yaw oscillations, normalized for size ($\sim l$), accelerations should be similar in magnitude, forces should scale as $m \sim l^3$, and eigenvalues should remain constant, implying identical stability properties in that perturbations are damped at the same rate per stride. Thus only $|F|$ among our performance measures varies – $|\lambda|, |\delta|$ and $|\theta|$ remain constant. This is summarized in column 1 of Table 1.

Blickhan and Full (1993) and Farley et al. (1993) observe that the sagittal-plane monopode should exhibit similarity of nondimensional 'relative stiffness' over a broad range of animals and adduce data supporting this. We likewise argue that the nondimensional parameters of (2) should occupy limited ranges, regardless of body geometry. We now estimate these ranges, and then explain the effects on gait of variations in individual physical parameters.

$\tilde{I}$ ranges. Allowable ranges of $\tilde{I}$ can be estimated by taking the moment of inertia of a uniform sphere of radius $R = \frac{l}{2}$ (a lady bug) to give a lower bound, and of a rod of length $4l$ (a stick insect) for an upper bound:

$$\tilde{I}_{\text{low}} \approx \frac{2}{5} m \left(\frac{l}{2}\right)^2 \cdot \frac{1}{ml^2} = 0.1, \qquad \tilde{I}_{\text{high}} \approx \frac{1}{12} m (4l)^2 \cdot \frac{1}{ml^2} = 1.33\ . \tag{5}$$

(Direct measurements for the death-head cockroach *Blaberus discoidalis* (Ting et al. 1994) yield the estimate $\tilde{I} = 0.82 \pm 0.2$.)

β and $\tilde{d}$ ranges. Both β and $\tilde{d}$ can be expected to vary within individual animals as they adjust stride length with speed, as well as across species (cf. Ting et al., and see Fig. 8). Since joint angle variations are generally constrained to 25–125° (McMahon 1975; Full and Ahn 1995; cf. McMahon 1984), values of β of 0.6–1.2 radians seem reasonable. We initially assumed that since foot forces are approximately directed along the legs in certain insects (Full et al. 1991) and legs are attached near the COM, the effective pivot position is unlikely to stray far from the COM, suggesting that $|\tilde{d}|$ remains small, but evidence presented in Fig. 7e disputes this and it is therefore difficult to estimate $\tilde{d}$.

$\tilde{k}$ ranges. The parameter $\tilde{k}$ depends on mass, speed, effective leg length, and stiffness k, the latter being perhaps the most difficult to estimate. 'Order-zero' behavior of $\tilde{k}$ can be obtained as follows. Since forward progression is achieved by sequential pivoting about the feet, leg cycle frequency f_s is proportional to angular velocity about the stance foot. Following Blickhan and Full (1993) and taking the linear spring approximation $f_s \approx \sqrt{k/m}$, we find

$$\sqrt{\frac{k}{m}} \cdot \frac{l}{v} = \sqrt{\tilde{k}} \approx \text{const.}\ , \tag{6}$$

although this neglects the effective potential due to conservation of momentum about the stance foot, which causes effective stiffening and frequency increase, and the fact that COM velocity v does not remain normal to the leg (Fig. 4). An upper bound on admissible magnitudes can be obtained by computing the critical $\tilde{k}_c$ above which steady gaits do not exist. We find $\tilde{k}_c \sim (\pi/2 - \beta)^{-2}$, with an increase from 1 to 9 as β varies from 0.6 to 1.2 radians (Schmitt and Holmes 2001). (For $\beta = \pi/2$ the leg is flung sideways, critical speed v_c drops to zero, and $\tilde{k}_c \to \infty$.)

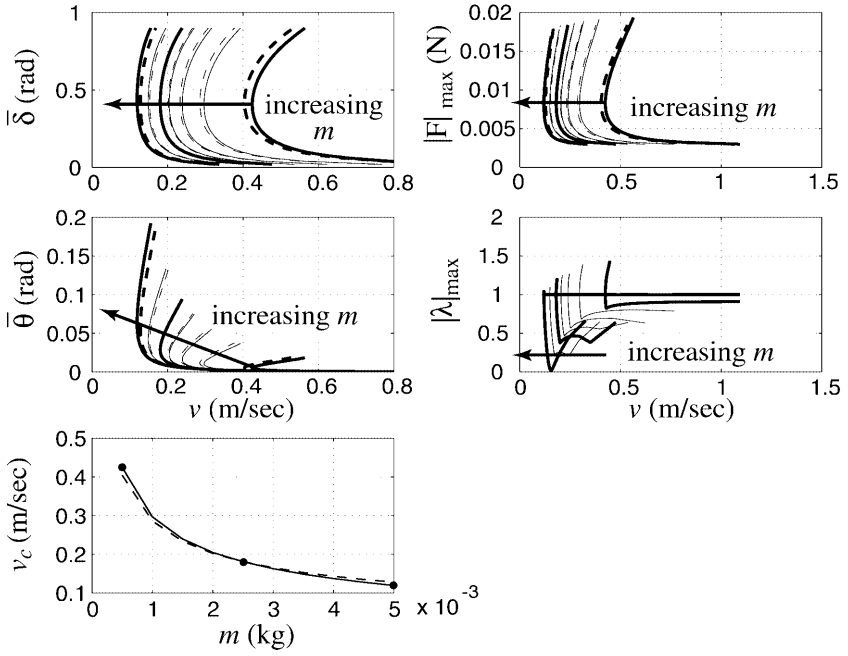

Fig. 9. Gait families for the moving-COP model with varying mass m; *solid curves*, numerical results; *dashed curves*, predictions from approximate scaling

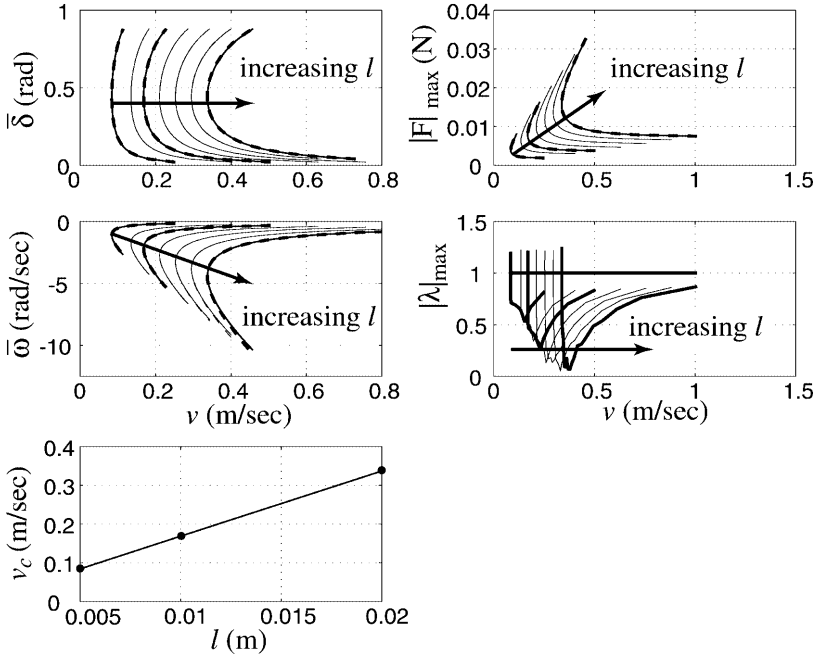

Fig. 10. Gait families for the fixed-COP model with varying leg length l; *solid curves*, numerical results; *dashed curves*, predictions from approximate scaling

5.2 Departures from geometric scaling: Individual parameter changes

As noted above, steady gaits for fixed $\tilde{\mu} = (\tilde{k}, \tilde{I}, \tilde{d}, \beta)$ follow identical paths, only differing via time rescaling. Thus, given a gait, Γ_1, for one set of physical parameter values, we can rescale to find the gait, Γ_2, for any other values which leave $\tilde{\mu}$ unchanged. We may use this device to predict gait scaling in response to individual parameter changes.

Effects of changes in stiffness k. Since k enters only $\tilde{k}$, we may keep $\tilde{\mu}$ constant by adjusting v alone, thereby incurring a timescale change to keep $\tilde{t}$ constant. Denoting variables for gaits Γ_1 and Γ_2 with appropriate subscripts, and proceeding as detailed in Schmitt and Holmes (2001), we compute the scale changes summarized in column 2 of Table 1. As k increases, the critical speed v_c and preferred speed increase, and forces at the preferred speed (based on optimal stability) increase. The other performance measures, including the maximum relevant eigenvalue, remain constant.

Effects of changes in mass m. Changes in mass leave $\tilde{\mu}$ unchanged only if v and I are *simultaneously* adjusted. However, for small $\tilde{d}$, the first (translational) equation of (1) is only weakly influenced by the second (rotational) equation. We may therefore allow $\tilde{I}$ to change with m,

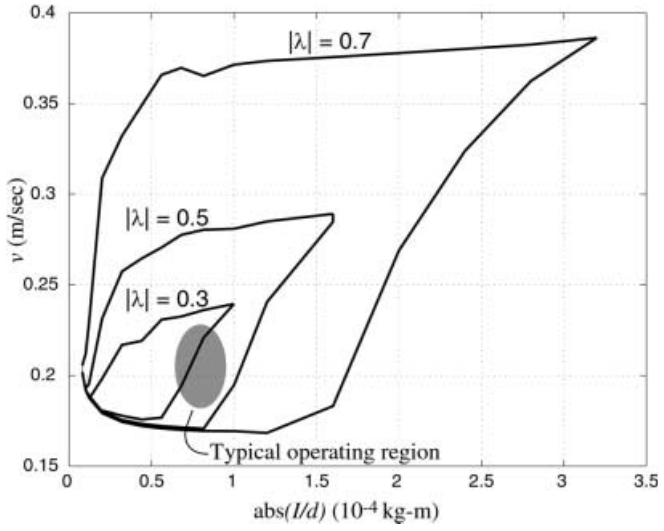

Fig. 11. Effects of changes in $|I/d|$ on stability. Forward speed $\langle v \rangle$ ranges over which gaits with a specified stability exit (maximum $|\lambda| < 1$ having the value indicated), decrease as $|I/d|$ becomes small or large. Eigenvalue magnitude contours computed for a fixed-COP model with $d = -0.0025$ m. The typical operating region for *Blaberus* (assuming $d = -0.0025$ m) – inferred from measurements of Kram et al. (1997) — is shown in *gray*

holding I fixed, and need only compensate yaw angle θ and angular velocities via $\theta_2/\theta_1 \approx \tilde{I}_1/\tilde{I}_2 = m_2/m_1$ cf. the second equation of (1). This leads to the approximate scale changes summarized in column 3 of Table 1. Here, an increase in mass leads to decrease in critical and preferred speeds, and in yaw angles and angular velocities at the preferred speed, and eigenvalue magnitudes decrease at rescaled speeds. See Fig. 9 for an example of how gait families transform under this scaling.

Effects of changes in leg length l. Changes in leg length leave $\tilde{\mu}$ unchanged only if v, I, and d are *all* adjusted, but again we may obtain an approximate scaling relation by compensating yaw angles to account for the fact that the nondimensional moments causing yawing are proportional to $\tilde{d}$. Thus $\theta_2/\theta_1 \approx \tilde{I}_1\tilde{d}_2/\tilde{I}_2\tilde{d}_1 = l_2/l_1$, and we obtain the approximate scaling summarized in column 4 of Table 1. (Note that the timescale does not change in this case, since $\tilde{t} = v_1 t_1/l_1 = v_2 t_2/l_2$, but that all dimensional quantities involving lengths are affected.) See Fig. 10 for an example. Here, increases in l cause increases in critical and preferred speeds, as well as increases in forces, yaw angles, and angular velocities at the preferred speed; however, eigenvalue magnitudes decrease at rescaled speeds.

These figures illustrate that the approximate scaling relations are acceptable (the maximum error is 8.8% in these cases). As expected, stiffness scaling predictions are exact, and an analog of Figs. 9 and 10 simply shows gait curves translated horizontally, with the exception of forces which increase with k. Further details and examples are given in Schmitt and Holmes (2001).

Effects of changes in I and d. We do not develop scaling laws for I and d individually, since, for small d, these parameters have little effect on translation dynamics and hence on critical velocity v_c, or on δ versus v gait curves. Their main effects are on yaw angle, θ, rate, ω, and stability, via the ratio I/d (or equivalently $\tilde{I}/\tilde{d}$). Low I/d promotes 'lively' yawing behavior, with a Hopf bifurcation (Guckenheimer and Holmes 1983) apparently occurring at a critical speed value, with oscillatory instability above this speed (although we have seen this only for $\tilde{I}/\tilde{d} < 0.32$, a range in which it is very difficult to find the fixed points). For high I/d the behavior is 'sluggish,' with $\omega \approx$ constant and the angular velocity eigenvalue approaching 1, as in the limiting case $d = 0$. For each speed in the admissible range, there is thus an optimal I/d value for which the stability performance measure $|\lambda|$ is minimized, much as a minimum emerges as a function of speed in the constant physical parameter gait families of Figs. 3, 9, and 10. Figure 11 illustrates this, showing a contour plot of eigenvalue magnitudes over the I/d-speed ($\langle v \rangle$) plane, with regions indicated in which the stability eigenvalues are *at least* as small in magnitude as the values shown.

The effects of these physical parameters on the performance measures and preferred speed V are summarized in Table 1. Note that the COM-velocity heading angle δ remains fixed under all specified parameter changes, but that stability properties, via $|\lambda|$, change with m, l, and I/d, as does the speed at which maximal stability is obtained (Fig. 11).

6 Discussion

In this paper we have described a simple three-degree-of-freedom mechanical model for the horizontal plane dynamics of rapidly running legged animals. The leg(s) involved in each stance phase are modeled by a single virtual or effective passive elastic member, the 'foot' of which is set in contact with the ground according to a preset feedforward protocol. The resulting bipedal LLS model exhibits asymptotically stable periodic gaits – similar to those of insects – over a range of forward speeds.

One of our major findings is that the LLS model belongs to a class of mechanical models for which neural or other detailed feedback is not necessary for stability. The purely mechanical effect of angular momentum transfer from foot to foot can produce strong asymptotic stability of COM heading and body angular velocity. The moments involved in this process are primarily due to lateral forces generated at the feet, indicating that lateral and yaw oscillations, which might seem inefficient, are *necessary* for stable gaits. (In Schmitt and Holmes (2001) we show that a model in which prescribed foot forces are not allowed to rotate with the body during stride has only *unstable* gaits.) In mechanics terms, for piecewise holonomic models such as this one, the stability is associated with the globally nonholonomic nature of the system (Ruina 1998), which arises from intermittent foot constraints. Since the model conserves energy and has no directional sensing, its speed and orientation are only neutrally stable: after perturbation, straight running resumes at a new angle and speed.

We also find that the stability properties vary over the allowable speed range for which gaits exist, and that a stability optimum occurs, corresponding to maximal decay rate for perturbations in heading and angular (yawing) velocity. This suggests a preferred speed based on stability considerations. For the case of the cockroach, this minimum falls in the observed range of preferred speeds.

In spite of its extreme simplicity and idealization (e.g., the assumption of energy conservation), the model, with appropriate parameter choices, reproduces with acceptable accuracy the horizontal-plane translational forces and velocity variations observed in running cockroaches at the preferred speed. Due to the collapse of the stance support tripod to a single virtual leg, however, moments and yaw variations are significantly underestimated. The animal evidently has greater flexibility in generating large moments without large net forces, than a model with only a single effective leg along which forces are supposed to act. This may be important in rapid turning, and there is evidence (Jindrich and Full 1999) that cockroaches adjust their individual foot forces in such maneuvers. In this regard, we have shown (Schmitt and Holmes 2000a) that both the fixed- and moving-COP models can execute realistic turns if one allows transient (positive) changes in the parameter d – during stance – on the leg opposite to the desired turn: such changes model 'favoring the front outside leg.'

We conclude that the LLS model can reproduce and help explain several aspects of locomotion dynamics in cockroaches. It lends support to our conjecture that the primary task of the neural central pattern generator in fast running might be to 'set the pace' and determine long-term heading and speed, leaving body mechanics to take care of stability in the short term (also see Full and Koditschek 1999). Moreover, we believe that this model can assist in understanding motion control in rapidly running animals more generally. Our scaling and parameter studies provide a basis for work, already in progress, to estimate parameters for running and walking animals over a range of sizes and shapes and to determine the extent to which: (1) the LLS model can qualitatively predict their behavior and (2) in particular how various parameters scale with size and gait style.

This work also provides a basis for more realistic modeling, incorporating multiple legs and/or better virtual leg specifications, active as well as passive joint torques and stiffnesses to better represent muscle groups, and models of sensory feedback and neural control. For example, inclusion of energy losses via dissipation, and its replenishment via muscle action, enables speed selection and speed stabilization (Schmitt J and Holmes P, unpublished work, 2002). In this and other cases, the conservative model can form an armature on which detail can be wound; in the terms of Full and Koditschek (1999), it provides a template for more detailed and realistic models to build on.

Acknowledgements. This work was supported by the US Department of Energy (DoE): DE-FG02-95ER25238 and DARPA/ONR: N00014-98-1-0747. Roberto Razo benefitted from a DoE GAANN grant: P-200-A80804. John Schmitt held a US Department of Defense Graduate Fellowship and a Wu Fellowship of the School of Engineering and Applied Science, Princeton University.

References

Anderson B (2000) Mechanics of a myriapod metachronal gait: legged locomotion in the laterally undulating arizona centipede, *Scolopendra heros*. PhD thesis, University of California, Berkeley, Calif.

Blickhan R, Full RJ (1987) Locomotion energetics of the ghost crab: II. Mechanics of the centre of mass during walking and running. J Exp Biol 130:155–174

Blickhan R, Full RJ (1993) Similarity in multi-legged locomotion: bouncing like a monopode. J Comp Physiol 173:509–517

Farley C, Glasheen J, McMahon TA (1993) Running springs: speed and animal size. J Exp Biol 185:71–86

Farley C, Gonzalez O (1996) Leg stiffness and stride frequency during human running. J Biomech 29:181–186

Farley C, Morgenroth D (1999) Leg stiffness primarily depends on ankle stiffness during hopping. J Biomech 32:267–273

Full RJ, Ahn AN (1995) Static forces and moments generated in the insect leg: comparison of a three-dimensional musculoskeletal computer model with experimental measurements. J Exp Biol 198:1285–1298

Full RJ, Koditschek DE (1999) Templates and anchors: neuromechanical hypotheses of legged locomotion on land. J Exp Biol 202:3325–3332

Full RJ, Tu MS (1990) Mechanics of six-legged runners. J Exp Biol 148:129–146

Full RJ, Tu MS (1991) Mechanics of a rapid running insect: two-, four- and six-legged locomotion. J Exp Biol 156:215–231

Full RJ, Blickhan R, Ting LH (1991) Leg design in hexpedal runners. J Exp Biol 158:369–390

Guckenheimer J, Holmes P (1983) Nonlinear oscillations, dynamical systems, and bifurcations of vector fields. Springer, Berlin Heidelberg New York

Hill AV (1950) The dimensions of animals and their muscular dynamics. Sci Prog 38:209–230

Jindrich D, Full RJ (1999) Many-legged maneuverability: dynamics of turning in hexapods. J Exp Biol 202:1603–1623

Kram R, Wong B, Full RJ (1997) Three-dimensional kinematics and limb kinetic energy of running cockroaches. J Exp Biol 200:1919–1929

Kubow TM, Full RJ (1999) The role of the mechanical system in control: a hypothesis of self-stabilization in hexapedal runners. Philos Trans R Soc Lond B 354:849–861

McMahon TA (1975) Using body size to understand the structural design of animals: quadrupedal locomotion. J Appl Physiol 39: 619–627

McMahon T (1984) Muscles, reflexes and locomotion. Princeton University Press, Princeton, N.J.

McMahon TA, Bonner J (1983) On size and life. Scientific American Books/W.H. Freeman, New York

McMahon TA, Cheng GC (1990) The mechanics of running: how does stiffness couple with speed? J Biomech 23 [Suppl 1]:65–78

Meriam JL, Kraige LG (1997) Engineering mechanics: dynamics, 4th edn. Wiley, New York

Ruina A (1998) Non-holonomic stability aspects of piecewise holonomic systems. Rep Math Phys 42:91–100

Schmitt J, Holmes P (2000a) Mechanical models for insect locomotion: dynamics and stability in the horizontal plane – application. Biol Cybern 83:517–527

Schmitt J, Holmes P (2000b) Mechanical models for insect locomotion: dynamics and stability in the horizontal plane – theory. Biol Cybern 83:501–515

Schmitt J, Holmes P (2001) Mechanical models for insect locomotion: stability and parameter studies. Physica D 156:139–168

Ting LH, Blickhan R, Full RJ (1994) Dynamic and static stability in hexapedal runners. J Exp Biol 197:251–269